Journal of Power Sources 195 (2010) 7011–7024

Contents lists available at ScienceDirect

Journal of Power Sources

journal homepage: www.elsevier.com/locate/jpowsour

Mass transport analysis of a passive vapor-feed direct methanol fuel cell

Chao Xu, Amir Faghri*

Department of Mechanical Engineering, University of Connecticut, Storrs, CT 06269, USA

ARTICLE INFO

Article history:
Received 2 March 2010
Received in revised form 29 April 2010
Accepted 4 May 2010
Available online 7 May 2010

Keywords:
Fuel cell
Passive DMFC
Vapor feed
Two-phase mass transport model
Water transport
Concentrated solution

ABSTRACT

A two-dimensional, two-phase, non-isothermal model using the multi-fluid approach was developed for a passive vapor-feed direct methanol fuel cell (DMFC). The vapor generation through a membrane vaporizer and the vapor transport through a hydrophobic vapor transport layer were both considered in the model. The evaporation/condensation of methanol and water in the diffusion layers and catalyst layers was formulated considering non-equilibrium condition between phases. With this model, the mass transport in the passive vapor-feed DMFC, as well as the effects of various operating parameters and cell configurations on the mass transport and cell performance, were numerically investigated. The results showed that the passive vapor-feed DMFC supplied with concentrated methanol solutions or neat methanol can yield a similar performance with the liquid-feed DMFC fed with much diluted methanol solutions, while also showing a higher system energy density. It was also shown that the mass transport and cell performance of the passive vapor-feed DMFC depend highly on both the open area ratio of the vaporizer and the methanol concentration in the tank.

1. Introduction

The direct methanol fuel cell (DMFC) is a promising portable power source for mobile electronic devices such as laptops, cellular phones, and PDAs, because of its advantages including easy fuel storage, high energy density, low temperature operation and compact structure. In spite of these advantages, the commercialization of DMFCs is still hindered by several technological obstacles: low active catalyst for methanol oxidation, methanol crossover through the membrane, mass transport, and water management [1–4]. The problem of methanol crossover is detrimental to the cell performance, as methanol crossover can not only result in a mixed potential on the cathode and thus lower the cell voltage, but it can also lead to wasted fuel, lowering the fuel efficiency. The rate of methanol crossover is strongly dependent of the methanol concentration in the anode catalyst layer. Therefore, diluted methanol solutions (0.5–2 M) are typically fed to DMFCs so that the rate of methanol crossover can be reduced. However, operating the DMFC with high methanol concentrations is the future application direction, as it increases the volumetric energy density and discharging time of the DMFC system [4].

In DMFCs, liquid methanol solution is supplied to the system, and can be fed either actively or passively to the anode in liquid or vapor phase. The vapor-feed DMFC has potential over a liquid-feed system in several ways [5–10]: (i) it has the potential to have a higher operating temperature, increasing the reaction rates and power outputs; (ii) the mass transfer is enhanced; (iii) methanol crossover is relatively lower; and (iv) high concentrated methanol solutions are used. The active vapor-feed DMFC has been reported since the 1990s [5,11–16]. It usually utilizes an electric heater or vaporizer at elevated temperatures between 130 °C and 200 °C in order to vaporize the liquid methanol solution, and then actively feed the mixture of water vapor and methanol vapor into the fuel cell for the reaction. However, this type of active vapor-feed DMFC has some critical disadvantages, including: (i) this vapor-phase operation at higher temperature requires more peripheral devices, such as the electric vaporizer, which lead to a complex structure and reduce the total system efficiency [8]; (ii) high operating temperatures (>90 °C) are required to avoid the condensation of the vapor mixture within the DMFC and achieve high cell performance; and (iii) methanol vapor in the anode exhaust is difficult to separate from the other gases. Accordingly, the active vapor-feed DMFC is incompatible with the need for portable applications.

Recently, the passive vapor-feed DMFC that operates at ambient temperature emerged as a promising DMFC technology for mobile power sources [6–9,17–29]. In contrast to the active vapor-feed DMFC, a passive vapor-feed DMFC does not need any device which consumes additional energy, such as the electric vaporizer. It typically utilizes a simple vaporizer to vaporize liquid methanol solution in the methanol tank: the methanol vapor is then passively transported to the DMFC anode. The methanol vapor may then condense to be liquid methanol solution in the anode of the passive vapor-feed DMFC. The anodic reaction may take place mainly in liquid phase, while it takes place in vapor phase in the active vapor-feed DMFC. Ren et al. [23,24] developed a passive vapor-feed DMFC, where both the passive fuel delivery system and the pas-

* Corresponding author. Tel.: +1 860 486 0419; fax: +1 860 486 0479.
E-mail address: faghri@engr.uconn.edu (A. Faghri).

0378-7753/$ – see front matter © 2010 Elsevier B.V. All rights reserved.
doi:10.1016/j.jpowsour.2010.05.003

Nomenclature

A_{lg}	interfacial specific area between liquid and gas phase ($m^2\ m^{-3}$)
A_v	specific area ($m^2\ m^{-3}$)
a_w	water vapor activity
C	molar concentration ($mol\ m^{-3}$)
c_p	specific heat capacity ($J\ kg^{-1}\ T^{-1}$)
D	diffusivity ($m^2\ s^{-1}$)
F	Faraday constant, 96,478 C mol^{-1}
Gr	Grashof number
h	heat transfer coefficient ($W\ m^{-1}\ K^{-1}$); Enthalpy ($J\ mol^{-1}$)
h_{lg}	interfacial transfer rate constant for methanol, $m^2\ s^{-1}$
h_m	mass transfer coefficient ($m^{-2}\ s^{-1}$)
I	current density ($A\ m^{-2}$)
I_p	parasitic current resulting from methanol crossover ($A\ m^{-2}$)
J	molar flux ($mol\ m^{-2}\ s^{-1}$)
j_0	exchange current density ($A\ m^{-2}$)
j_a	anode current density ($A\ m^{-3}$)
j_c	cathode current density ($A\ m^{-3}$)
K	permeability of porous material (m^2); partition coefficient
k	thermal conductivity ($W\ m^{-1}\ K^{-1}$)
k_c	condensation rate ($mol\ (atm\ s\ m^3)^{-1}$)
k_e	evaporation rate $(atm\ s)^{-1}$
k_r	relative permeability
L	the vaporizer thickness (m)
$\dot{m}$	source term in mass conservation equation ($kg\ m^{-3}\ s^{-1}$)
M	molecular weight ($kg\ mol^{-1}$)
N	mol flux ($mol\ m^{-2}\ s^{-1}$)
Nu	Nusselt number
n_d	electro-osmotic drag coefficient
p_c	capillary pressure (Pa)
p_g	gas phase pressure (Pa)
p_l	liquid phase pressure (Pa)
Pr	Prandtl number
R	gas constant $(J\ (mol\ K)^{-1})$
$\dot{R}$	source term in species conservation equation ($mol\ m^{-3}\ s^{-1}$)
$\tilde{R}$	interfacial species transfer rate ($mol\ m^{-3}\ s^{-1}$)
$R_{contact}$	ohmic contact resistance ($\Omega\ m^2$)
S	source term; entropy
Sc	Schmidt number
Sh	Sherwood number
s	liquid saturation; entropy
T	temperature (K)
V_0	thermodynamic equilibrium voltage (V)
V_{cell}	cell voltage (V)
x	coordinate (m)
y	coordinate (m)

Greek symbols

α_a	anode transfer coefficient at anode
α_c	cathode transfer coefficient at cathode
γ	reaction order of ORR
δ	thickness of porous layer (m)
ε	porosity of porous medium
η	overpotential (V)
λ	water content
μ	viscosity ($kg\ m^{-1}\ s^{-1}$)
ρ	density ($kg\ m^{-3}$)
σ	interfacial tension ($N\ m^{-1}$); proton conductivity ($\Omega^{-1}\ m^{-1}$)

Superscripts

eff	effective value
ref	reference value
sat	saturated value
*	in equilibrium
∞	values in ambient air

Subscripts

a	anode
c	cathode, or capillary
cr	crossover
dry	dry membrane
e	electrolyte, or evaporation
g	gas phase
l	liquid phase
mem	membrane
ML	methanol
MV	methanol vapor
p	parasitic
pm	pervaporation membrane
rl	relative value for liquid phase
rg	relative value for gas phase
T	temperature
tank	methanol tank
vapor	water vapor
W	water
we	dissolved water
WV	water vapor

sive water management system were presented. They introduced a pervaporation membrane (silicone membrane) as a vaporizer, and optimized the cathode structure to achieve the water supply from the cathode to the anode by back diffusion and back convection. Kim et al. [9,25] developed a semi-passive DMFC which was fueled by methanol vapor. Liquid methanol was supplied to the porous foam by a syringe pump. Methanol was vaporized through a membrane vaporizer (Nafion 112), and then diffused through a water barrier layer and a buffer layer to get to the anode electrode. The vapor-feed DMFC system was able to run for 360 h between 20 and 25 mW cm^{-2}, and performed with a 70% higher fuel efficiency and 1.5 times higher energy density compared with the liquid-feed system. Guo and Faghri [17,29] presented a novel vapor-feed DMFC with a passive thermal-fluids management system. Pure methanol was wicked from a reservoir to a porous evaporation pad where methanol was vaporized. It was shown that a heat source was critical for the effective operation of the fuel cell system since water condensation on the methanol evaporation pad can limit the operating time. In practice, heat source can be obtained by wasted heat using heat pipes. Eccarius et al. [7,8] recently investigated the impacts of structure parameters and operating conditions for a passive vapor-feed DMFC. The methanol vapor was generated with a polydimethylsiloxane (PDMS) pervaporation membrane, and the evaporation rate of methanol into the vapor chamber was controlled by different open area ratios of a solid plate attached to the PDMS membrane. It was found that water management was a critical parameter for a passive vapor-feed DMFC, and a microstructured cathode electrode was used to increase water back diffusion from the cathode to the anode.

Besides experimental investigation, mathematic modeling about DMFCs plays an important role, as it can provide a powerful

and economical tool to quantify the complex transport and electrochemical phenomena, as well as optimize the cell design and operation conditions [30,31]. Extensive efforts have been made to develop numerical models for liquid-feed DMFCs [30–36]. However, only two modeling work about the passive vapor-feed DMFC has been reported [10,27]. Rice and Faghri [10] first developed a one-dimensional analysis of the transport of methanol from the fuel source to the fuel cell, and then investigated the fundamentals of the passive vapor-feed DMFC using a transient, two-dimensional, two-phase thermal model. The results showed that water management in a passive vapor delivery system was crucial in the fuel cell, as well as in the methanol distribution layer. However, the vapor generation process through the vaporizer was not considered in the model. Xiao and Faghri [27] later investigated the transient and polarization characteristics of a passive vapor-feed DMFC using a transient, two-dimensional, multiphase model. The evaporation/condensation phenomenon at the vaporizer was considered, but the methanol and water vapor concentrations across the vapor chamber were assumed to be constant. Both of the two models employed an equilibrium assumption between species (methanol and water) in liquid and gas phases.

The objective of the present work is to seek the fundamental understanding of the mass transport in the passive vapor-feed DMFC, which is essential for the performance improvement and cell design of the fuel cell system. First, the physical principle of the passive vapor-feed DMFC was discussed, and the difference with the liquid-feed DMFC was shown. Then, a two-dimensional, two-phase, non-isothermal model for the passive vapor-feed system using the multi-fluid approach was developed. The vapor generation process through the vaporizer and the vapor transport through the vapor transport layer were both considered in the model. With this model, the working process of the passive vapor-feed DMFC, as well as the effects of various operating parameters and cell configurations on the mass transport and cell performance, was studied.

2. Physical principle of the passive vapor-feed DMFC

The working physical principle of the passive vapor-feed DMFC can be elucidated by referring to the anode side illustrated in Fig. 1a. It is seen that concentrated methanol solution or neat methanol directly contacts one side of the vaporizer, through which methanol vapor is generated due to the high-volatility of liquid methanol. The vaporizer can be a pervaporation membrane [7–9,23,24] or a heated porous pad [17]. A vapor transport layer (VTL) which is attached on the other side of the vaporizer is usually needed. The VTL is a hydrophobic porous layer which is used to transport the methanol vapor to the anode diffusion layer (DL) of the DMFC and simultaneously to prevent liquid transport through it. In the anode DL and catalyst layer (CL), due to the presence of hydrophilic pores [10,32] and the relatively low operating temperature, methanol vapor is prone to condense to the liquid phase. If liquid water generated at the cathode can be partially recovered to the anode side through the membrane, the condensation of methanol vapor will lead to the formation of diluted methanol solution in the anode DL and CL. Then methanol in solution is transported through the anode DL to the catalytic sites in the CL, on which the electrochemical oxidation of methanol takes place. It is noted that the contribution of the anodic reaction taking place in the vapor phase is assumed to be negligible at room temperature operation due to the very low kinetics and low activity. Besides, part of the methanol will permeate through the membrane to the cathode side due to the concentration difference, and hence, will lower the cell performance due to the mixed-potential at the cathode.

When neat methanol is fed to the vapor-feed DMFC, for the first several minutes, no current can be discharged since no water

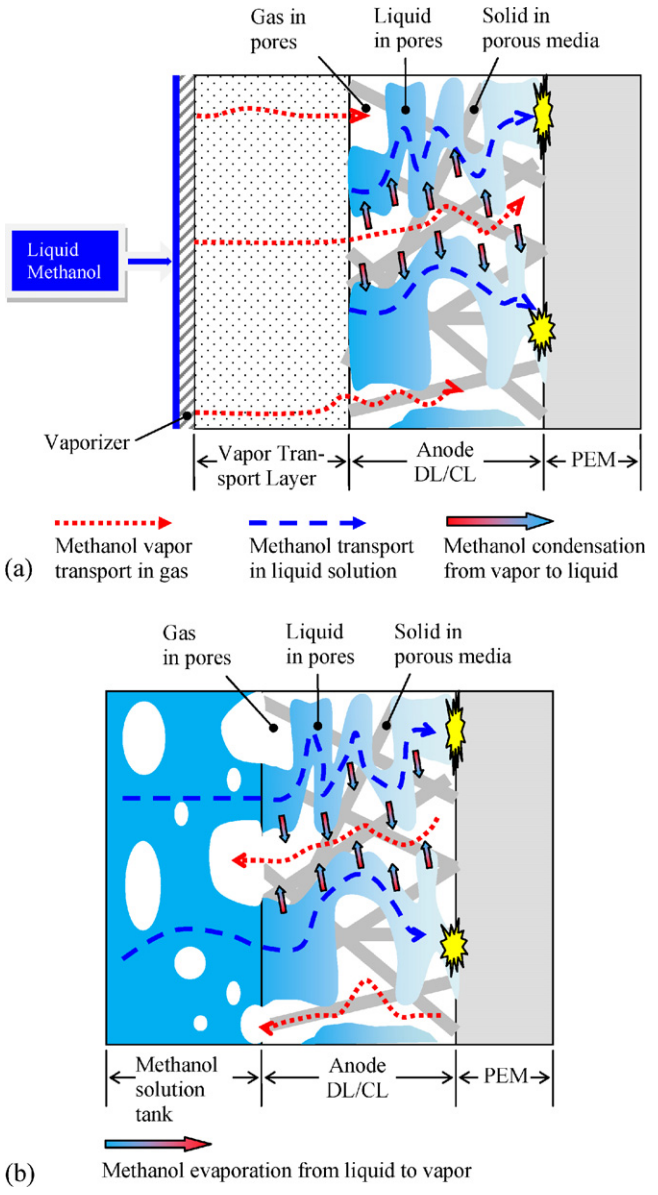

Fig. 1. Illustration of (a) the passive vapor-feed DMFC anode, and (b) the passive liquid-feed DMFC anode.

exists in the anode (the anodic reaction cannot take place). After methanol arrives at the cathode through the membrane, water will be generated from the reaction of methanol and oxygen with the help of the Pt catalysts. The produced water in the cathode can permeate through the membrane to the anode and take part in the anodic reaction. Therefore, in the vapor-feed DMFC fed with neat methanol, water needed for the anodic reaction is completely recovered from water generated at the cathode.

Clearly, in terms of the cell structure, the passive vapor-feed DMFC has only an additional membrane vaporizer and a hydrophobic VTL compared to the passive liquid-feed DMFC. The thickness of the additional layers can be very thin, e.g., ~0.1–0.3 mm and ~0.5–2 mm for the vaporizer and the VTL, respectively, which brings little penalty in terms of the volumetric energy density of the system. As thus, the passive vapor-feed DMFC has some specific advantages such as: compact structure, low operation temperature, and high volumetric energy density (direct use of highly concentrated methanol solution or neat methanol).

To further clarify the working principle of the passive vapor-feed DMFC, it is worth comparing it with the liquid-feed DMFC,

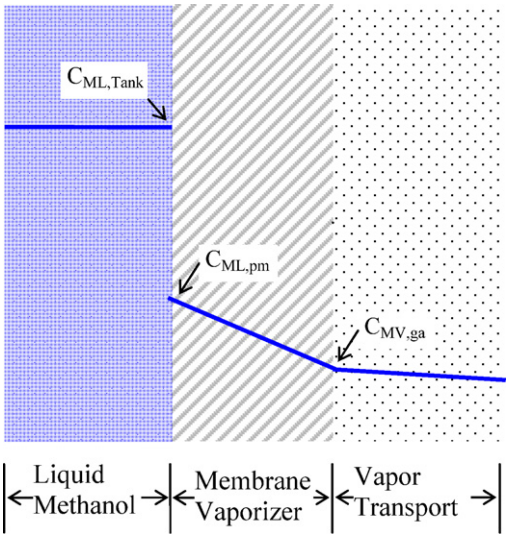

Fig. 2. Scheme of the pervaporation process of liquid methanol through the membrane vaporizer.

the anode side of which is illustrated in Fig. 1b. In the anode of the liquid-feed DMFC, liquid methanol in the diluted methanol solution is transported from the solution tank through the DL to the CL, where part of it reacts with water to form gas CO_2. In the meantime, the produced gas CO_2 in the CL is transported backward through the DL to the tank, and is vented out through the CO_2 exit. Therefore, liquid–gas two-phase flow occurs in both the passive vapor-feed DMFC and the liquid-feed DMFC. For the two types of DMFC, the electrochemical oxidation reaction of methanol all takes place mainly in liquid phase. However, there are some differences between the vapor-feed and liquid-feed DMFCs. First, diluted methanol solution is directly fed to the liquid-feed DMFC, while for the vapor-feed DMFC, concentrated methanol solution or neat methanol is supplied to the methanol tank, and then after vaporization, the methanol vapor is fed to the anode. As thus, there is no liquid flux through the surface of the anode DL in the vapor-feed DMFC. Second, in the liquid-feed DMFC, liquid methanol vaporizes from the diluted solution into the gas phase with the removal of gas CO_2, while in the vapor-feed DMFC, methanol vapor condenses to form diluted methanol solution in the anode DL and CL. Third, in the liquid-feed DMFC, water needed for the anodic reaction may be directly supplied from the fed diluted methanol solution, while in the passive vapor-feed DMFC, water needed in the anode needs to be recovered from the cathode.

Since most previous experimental work about the passive vapor-feed DMFC utilized pervaporation membranes as the vaporizer [7–9,23,24], this numerical analysis is also based on a pervaporation membrane. The pervaporation process of liquid methanol through the membrane vaporizer is illustrated in Fig. 2. Based on the solution-diffusion model, assuming the transport resistance is mainly through the membrane vaporizer, the flux of methanol through the membrane can be approximately expressed as [37]:

$$J_{MV} = \frac{C_{ML,pm}}{L} D_{pm}(1 - C_{MV,ga}\big|_{+} RT/p_{b,Tank}) \quad (1)$$

where $C_{ML,pm}$ is the methanol concentration in the membrane at the liquid-membrane interface, D_{pm} the diffusion coefficient in the pervaporation membrane, L the pervaporation membrane thickness, $p_{b,Tank}$ the pressure of methanol tank, and $C_{MV,ga}\big|_{+}$ the concentration of methanol vapor at the membrane-vapor interface. $C_{ML,pm}$ can be conveniently correlated to the methanol concentration in the tank ($C_{ML,Tank}$) with the partition coefficient of the methanol in both liquid and membrane: $K = C_{ML,pm}/C_{ML,Tank}$.

It is worth noting that the total flux of methanol through the membrane also depends on the effective area of the pervaporation membrane facing the VTL, which can be controlled by adding a thin perforated layer with an open area ratio of A between the membrane and the VTL [7,8]. The open area ratio is defined as the perforated area to the active area of the MEA. Thus, the flux of methanol through the membrane vaporizer can be expressed as:

$$J_{MV} = \frac{AC_{ML,Tank}}{L} D_{pm} K(1 - C_{MV,ga}\big|_{+} RT/p_{b,Tank}) \quad (2)$$

From the above equation, it is clear that for a given methanol concentration in the tank ($C_{ML,Tank}$), the vapor generation rate from the membrane vaporizer (J_{MV}), as well as the concentration of methanol vapor at the membrane-vapor interface ($C_{MV,ga}\big|_{+}$), can be controlled by the membrane thickness (L) and the open area ratio of the vaporizer (A).

3. Model formulation

Consider a two-dimensional physical domain, as illustrated in Fig. 3, which represents a passive vapor-feed DMFC that consists of a liquid fuel tank, a membrane vaporizer, a hydrophobic porous VTL, an anode DL and CL, a membrane, a cathode CL and DL, and a hydrophobic porous air filter layer (AFL). The AFL also works as a water-blocking layer, which is necessary in future commercial applications since no liquid is expected to leak through the cathode side. As shown in previous investigations [31,32], the AFL is essential both to avoid direct liquid water loss from the cathode to the ambient air and to achieve an interior water recovery from the cathode through the membrane to the anode. In the following, the model to formulate the mass transport and heat transport in different regions of the computational domain is presented. The following main assumptions are made in the model: (i) the fuel cell operates under steady-state conditions; (ii) the porous layers are homogeneous and isotropic; (iii) both gas and liquid phases are continuous in porous layers; (iv) only water and methanol are considered as the condensable species; (v) the membrane is impermeable to both gases and liquid, and the crossover of methanol and water through the membrane is through dissolved phase; (vi) the liquid and gas phases' temperature are the same.

3.1. Governing equations for mass and heat transport

3.1.1. Mass transport in the anode porous region

The anode porous region includes the VTL, anode DL and anode CL. Since the hydrophobic VTL is used for blocking the liquid transport while still allowing for the vapor transport, it is assumed that only gas phase exists in the VTL. While in the anode DL and CL, both liquid phase and gas phase exist due to the coexistence of the hydrophilic and hydrophobic pores. The general governing equations of the mass and momentum conservation corresponding to each phase, as well as the conservation of species, are given by

$$\text{Mass}: \quad \nabla \cdot [\rho_l u_l] = \dot{m}_{l,a}\,(\text{Liquid phase}) \quad (3)$$

$$\nabla \cdot \left[\rho_g u_g\right] = \dot{m}_{g,a}\,(\text{Gas phase}) \quad (4)$$

where u represents the superficial velocity vector based on the total cross-sectional area of fluids and porous medium, and $\dot{m}$ is the mass generate rate.

$$\text{Momentum}: \quad u_l = -K\frac{k_{rl}}{\mu_l}\nabla p_{l,a}\,(\text{Liquid phase}) \quad (5)$$

$$u_g = -K\frac{k_{rg}}{\mu_g}\nabla p_{g,a}\,(\text{Gas phase}) \quad (6)$$

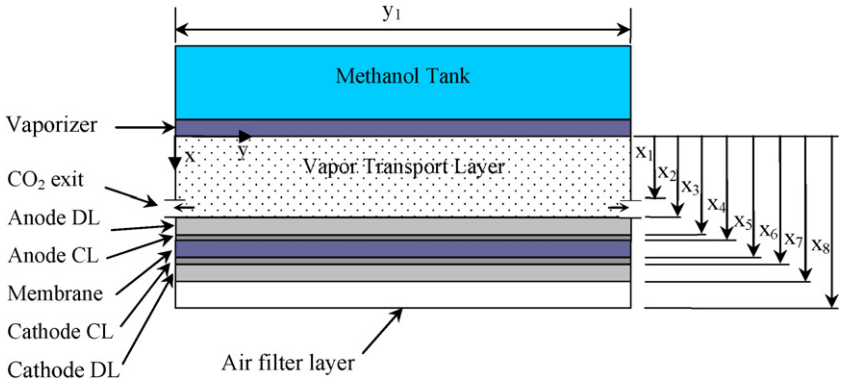

Fig. 3. Schematic of the model domain of the passive vapor-feed DMFC.

where K is the intrinsic permeability of the porous medium, and k_r denotes the relative permeability of a phase.

$$\text{Species}: \quad \nabla\cdot(u_l C_{ML,a}) = \nabla\cdot(D^{eff}_{ML,a}\cdot\nabla C_{ML,a}) + \dot{R}_{ML,a} \ \text{(Methanol in liquid)} \tag{7}$$

$$\nabla\cdot(u_g C_{MV,ga}) = \nabla\cdot(D^{eff}_{MV,ga}\cdot\nabla C_{MV,ga}) + \dot{R}_{MV,ga} \ \text{(Methanol in vapor)} \tag{8}$$

$$\nabla\cdot(u_g C_{WV,ga}) = \nabla\cdot(D^{eff}_{WV,ga}\cdot\nabla C_{WV,ga}) + \dot{R}_{WV,ga} \ \text{(Water vapor)} \tag{9}$$

where D_i^{eff} represents the effective diffusion coefficient of species i, and $\dot{R}_i$ denotes the mole generation rate of species i.

3.1.2. Mass transport in the cathode porous region

The cathode porous region includes the cathode CL, cathode DL and AFL. In the cathode DL and CL, both liquid phase and gas phase exist due to the coexistence of the hydrophilic and hydrophobic pores. Since liquid water cannot leak through the hydrophobic AFL to the ambient air, only gas phase exists in the AFL. The general governing equations of the mass and momentum conservation corresponding to each phase, as well as the conservation of species, are given by

$$\text{Mass}: \quad \nabla\cdot[\rho_l u_l] = \dot{m}_{l,c} \ \text{(Liquid phase)} \tag{10}$$

$$\nabla\cdot\left[\rho_g u_g\right] = \dot{m}_{g,c} \ \text{(Gas phase)} \tag{11}$$

$$\text{Momentum}: \quad u_l = -K\frac{k_{rl}}{\mu_l}\nabla p_{l,c} \ \text{(Liquid phase)} \tag{12}$$

$$u_g = -K\frac{k_{rg}}{\mu_g}\nabla p_{g,c} \ \text{(Gas phase)} \tag{13}$$

$$\text{Species}: \quad \nabla\cdot(u_g C_{O_2,gc}) = \nabla\cdot(D^{eff}_{O_2,gc}\cdot\nabla C_{O_2,gc}) + \dot{R}_{O_2,gc} \ \text{(Oxygen)} \tag{14}$$

$$\nabla\cdot(u_g C_{WV,gc}) = \nabla\cdot(D^{eff}_{WV,gc}\cdot\nabla C_{WV,gc}) + \dot{R}_{WV,gc} \ \text{(Water vapor)} \tag{15}$$

It should be noted that the difference between the pressures of gas phase and liquid phase in the two-phase regions is related to the capillary pressure, which is given by [32,38]:

$$p_c = p_g - p_l = d(\exp(-a_1[s-c]) - \exp(a_2[s-c])) + b \tag{16}$$

where $a_1 = -44.9$, $a_2 = -22.1$, $b = 35.6$ (Pa), $c = 0.321$ and $d = -2.09$ (Pa) for the DL, while $a_1 = -23.5$, $a_2 = -17.4$, $b = 477.0$ (Pa), $c = 0.46$ and $d = -3.58$ (Pa) for the CL. This capillary pressure relation was developed by Nguyen et al. [38] based on fuel cell diffusion media; it shows a mixed-wet behavior due to the coexistence of hydrophilic and hydrophobic pores in the fuel cell DL and CL [32,38].

3.1.3. Mass transport in the membrane

In the electrolyte membrane, only dissolved water and methanol need to be considered, as the membrane is regarded as a gas insulator due to its extremely low permeability. The transfer of dissolved water through the membrane depends on molecular diffusion, electro-osmotic drag, and convection. Accordingly, the molar flux of water crossover (N_{H_2Ocr}) through the membrane can be given by:

$$N_{H_2Ocr} = -D_{we}(\lambda)\nabla C_{we} + n_{d,H_2O}\frac{I}{F} - \frac{K_{mem}\rho_l}{\mu_l M_{H_2O}}\nabla p_l \tag{17}$$

Thus, the governing equation for the dissolved water concentration (C_{we}) is:

$$\nabla\cdot N_{H_2Ocr} = \nabla\cdot(-D_{we}(\lambda)\nabla C_{we}) + \nabla\cdot\left(n_{d,H_2O}\frac{I}{F}\right) = 0 \tag{18}$$

The molar flux of methanol crossover (N_{MLcr}) through the membrane, which also depends on molecular diffusion, electro-osmotic drag and convection, can be given by:

$$N_{MLcr} = -D_{M,N}\nabla C_{ML} + n_{d,M}\frac{I}{F} - \left(\frac{K_{mem}\Delta p_{l,c-a}}{\mu_l\delta_{mem}}\right)C_{ML} \tag{19}$$

where $\Delta p_{l,c-a}$ represents the liquid pressure difference between the cathode and the anode.

3.1.4. Heat transport

The energy equation used in the entire computational domain can be expressed as follows [31]:

$$\nabla\cdot(\rho_l c_{p,l}\vec{u}_l T) + \nabla\cdot(\rho_g c_{p,g}\vec{u}_g T) = \nabla\cdot(k_T^{eff}\nabla T) + S_T \tag{20}$$

where k_T^{eff} represents the effective thermal conductivity of heat transfer media, and S_T denotes the heat generation rate.

Up to this point, the mathematical formulation of the mass and heat transport processes in all the regions of the vapor-feed DMFC has been presented. The required constitutive correlations and associated nomenclatures are listed in Table 1.

3.2. Boundary and interfacial conditions

The conditions at each boundary/interface, in reference to Fig. 3, are described below.

$x = 0$: This boundary represents the interface between the membrane vaporizer and the VTL, through which liquid methanol vaporizes to be vapor. As discussed in the proceeding section, the generation rate of methanol vapor through the vaporizer can be expressed by Eq. (2). For the other variables, it is assumed that the vaporizer membrane is an insulator for gas transport, and thus the boundary conditions can be given

$$\frac{\partial\phi}{\partial x} = 0, \ \phi = p_{g,a}, C_{WV,ga} \tag{21}$$

$x = x_2$: This interface represents the contacting surface of the VTL and anode DL, through which liquid cannot penetrate, and thus the

Table 1
Constitutive relations in the governing equations.

Parameters	Expressions
Relative permeabilities [31]	$k_{rl} = s^{4.5}$ Liquid $k_{rg} = (1-s)^{4.5}$ Gas
Effective diffusion coefficients of species [33]	$D_{i,g}^{eff} = D_{i,g}\varepsilon^{1.5}(1-s)^{1.5}\ i: O_2, WV, MV$
	$D_{ML,a}^{eff} = \begin{cases} D_{M,l}\varepsilon^{1.5}s^{1.5} & \text{ADL} \\ \dfrac{(\varepsilon+\varepsilon_e)}{[\varepsilon/(D_{M,l}\varepsilon^{1.5}s^{1.5})+\varepsilon_e/(D_{M,N}\varepsilon_e^{1.5})]} & \text{ACL} \\ D_{M,N} & \text{PEM} \end{cases}$
Effective thermal conductivity in the porous regions [31]	$k_T^{eff} = \begin{cases} \varepsilon k_g + k_{VTL/AFL} & \text{VTL(AFL)} \\ \varepsilon s k_l + \varepsilon(1-s)k_g + k_{DL/CL} & \text{DL(CL)} \\ k_{mem} & \text{PEM} \end{cases}$
General generation rate of mass in liquid phase	$\dot{m}_{l,a} = \begin{cases} 0 & \text{VTL} \\ M_{H_2O}\tilde{R}_{vl} - M_M\tilde{R}_{MV,ga} & \text{ADL} \\ M_{H_2O}\left(\tilde{R}_{vl} - \dfrac{N_{H_2Ocr}}{\delta_{acl}} - \dfrac{j_a}{6F}\right) - M_M\left(\tilde{R}_{MV,ga} + \dfrac{j_a}{6F} + \dfrac{I_p}{6F\delta_{acl}}\right) & \text{ACL} \end{cases}$
	$\dot{m}_{l,c} = \begin{cases} 0 & \text{AFL} \\ M_{H_2O}\tilde{R}_{vl} & \text{CDL} \\ M_{H_2O}\left(\tilde{R}_{vl} + \dfrac{N_{H_2Ocr}}{\delta_{ccl}} + \dfrac{(j_c - I_p/\delta_{ccl})}{2F} + \dfrac{I_p}{3F\delta_{ccl}}\right) & \text{CCL} \end{cases}$
General generation rate of mass in gas phase	$\dot{m}_{g,a} = \begin{cases} 0 & \text{VTL} \\ -M_{H_2O}\tilde{R}_{vl} + M_M\tilde{R}_{MV,ga} & \text{ADL} \\ -M_{H_2O}\tilde{R}_{vl} + M_M\tilde{R}_{MV,ga} + M_{CO_2}\dot{R}_{CO_2,ga} & \text{ACL} \end{cases}$
	$\dot{m}_{g,c} = \begin{cases} 0 & \text{AFL} \\ -M_{H_2O}\tilde{R}_{vl} & \text{CDL} \\ -M_{O_2}j_c/4F + M_{CO_2}I_p/6F\delta_{ccl} - M_{H_2O}\tilde{R}_{vl} & \text{CCL} \end{cases}$
Mole generation rate of species	$\dot{R}_{O_2,gc} = \begin{cases} 0 & \text{AFL} \\ 0 & \text{CDL} \\ -j_c/4F & \text{CCL} \end{cases}, \dot{R}_{WV,gc} = -\tilde{R}_{vl}$
	$\dot{R}_{ML,a} = \begin{cases} 0 & \text{VTL} \\ -\tilde{R}_{MV,ga} & \text{ADL} \\ -\tilde{R}_{MV,ga} - j_a/6F & \text{ACL} \end{cases}$
	$\dot{R}_{WV,ga} = -\tilde{R}_{vl}, \dot{R}_{MV,ga} = \tilde{R}_{MV,ga}\ \text{(ADL/ACL)}$
Heat generation rate [31]	$S_T = \begin{cases} 0 & \text{VTL} \\ \tilde{R}_{vl}\Delta h_v - \tilde{R}_{MV,g}\Delta h_{Mv} & \text{ADL} \\ j_a(\eta_a - T\Delta S_{MOR}/6F) + I^2/\sigma_{mem}^{eff} + \tilde{R}_{vl}\Delta h_v - \tilde{R}_{MV,g}\Delta h_{Mv} & \text{ACL} \\ I^2/\sigma_{mem} & \text{PEM} \\ j_c(\lvert\eta_c\rvert - T\Delta S_{ORR}/4F) - I_pT\Delta S_{MOR}/6F\delta_{ccl} & \text{CCL} \\ \quad +I^2/\sigma_{mem}^{eff} + \tilde{R}_{vl}\Delta h_v & \\ \tilde{R}_{vl}\Delta h_v & \text{CDL} \\ 0 & \text{AFL} \end{cases}$

liquid flux and liquid methanol flux in the x-direction are zero:

$$\left.\frac{\partial C_{\mathrm{ML}}}{\partial x}\right|_{+}=0,\quad \left.\frac{\partial p_{\mathrm{l,a}}}{\partial x}\right|_{+}=0 \tag{22}$$

$x=x_4$: This interface is the interface between the anode CL and the membrane, which is impermeable for both the gas and the liquid. Thus, all of the fluxes except the dissolved water in the x-direction are:

$$\left.\frac{\partial p_{\mathrm{l,a}}}{\partial x}\right|_{-}=0,\quad \left.\frac{\partial p_{\mathrm{g,a}}}{\partial x}\right|_{-}=0,\quad \left.\frac{\partial C_{\mathrm{WV,ga}}}{\partial x}\right|_{-}=0,\quad \left.\frac{\partial C_{\mathrm{MV,ga}}}{\partial x}\right|_{-}=0,\quad \left.\frac{\partial C_{\mathrm{ML}}}{\partial x}\right|_{-}=0 \tag{23}$$

Note that the methanol crossover is considered by a uniform source term in the CL, since the dissolving process of methanol into the electrolyte occurs within the whole CL.

For the concentration of dissolved water in the electrolyte membrane, it is assumed that the water concentration at the surface of the membrane is in equilibrium with the water state in the porous region of the CL [39,40]. The dissolved water concentration (C_{we}) can be transformed to the water content (λ) in the electrolyte, and the relationship between the two is given by

$$\lambda=\frac{EW}{\rho_{\mathrm{dry}}}C_{\mathrm{we}} \tag{24}$$

When the Nafion membrane is in equilibrium with saturated water vapor, the water content in the membrane approaches an equilibrium value ($\lambda^*_{\mathrm{we,v}}$), which can be approximated by [30]

$$\lambda^*_{\mathrm{we,v}}=\lambda^*_{\mathrm{we,v_{@303\,K}}}+\frac{\lambda^*_{\mathrm{we,v_{@353\,K}}}-\lambda^*_{\mathrm{we,v_{@303\,K}}}}{50}(T-303) \tag{25}$$

where $\lambda^*_{\mathrm{we,v_{@353\,K}}}=0.3+10.8a_{\mathrm{w}}-16a_{\mathrm{w}}^2+14.1a_{\mathrm{w}}^3$, $\lambda^*_{\mathrm{we,v_{@303\,K}}}=0.043+17.81a_{\mathrm{w}}-39.85a_{\mathrm{w}}^2+36.0a_{\mathrm{w}}^3$, and a_{w} is the water vapor activity ($a_{\mathrm{w}}=x_{\mathrm{vapor}}p_{\mathrm{g}}/p^{\mathrm{sat}}_{\mathrm{vapor}}$). When the electrolyte Nafion is submerged in liquid water, its equilibrium water content appears to jump discontinuously to a higher value of $\lambda^*_{\mathrm{we,l}}=22$. Thus, for the equilibrium water content which is in equilibrium with the liquid-gas two phase mixture, a linear expression is used for an approximation as follows [30]:

$$\lambda^*_{\mathrm{we}}\big|_{+}=\lambda^*_{\mathrm{we,v}}+(\lambda^*_{\mathrm{we,l}}-\lambda^*_{\mathrm{we,v}})s|_{-} \tag{26}$$

where $s|_{-}$ is the liquid saturation in the surface of the anode CL facing the membrane.

$x=x_5$: This interface is the interface between the membrane and the cathode CL. It is assumed that the methanol permeated from the anode will be depleted immediately due to the fast methanol reaction at the cathode, and thus the methanol concentration at this interface is zero. Similar to interface at $x=x_4$, all the gas and liquid fluxes in the x-direction are also zero at this interface

$$C_{\mathrm{ML}}|_{-}=0,\quad \left.\frac{\partial p_{\mathrm{l,c}}}{\partial x}\right|_{+}=0,\quad \left.\frac{\partial p_{\mathrm{g,c}}}{\partial x}\right|_{+}=0,\quad \left.\frac{\partial C_{\mathrm{WV,gc}}}{\partial x}\right|_{+}=0,\quad \left.\frac{\partial C_{\mathrm{O_2,gc}}}{\partial x}\right|_{+}=0 \tag{27}$$

The dissolved water concentration in the membrane at this interface is also given by:

$$\lambda^*_{\mathrm{we}}\big|_{-}=\lambda^*_{\mathrm{we,v}}+(\lambda^*_{\mathrm{we,l}}-\lambda^*_{\mathrm{we,v}})s|_{+} \tag{28}$$

$x=x_7$: This interface is the interface between the cathode DL and AFL. As discussed in previous investigations [31,32], no liquid water can penetrate across the hydrophobic AFL, and thus the liquid flux in the x-direction is zero at this interface:

$$\left.\frac{\partial p_{\mathrm{l,c}}}{\partial x}\right|_{-}=0 \tag{29}$$

$x=x_8$: This boundary represents the surface of the AFL exposed to the ambient air. At this boundary, the mass transport of gases and heat transport between the surface and the ambient air are through natural convection. Thus, the following boundary conditions are specified by [31,32]

$$p_{\mathrm{g,c}}=p^{\infty}_{\mathrm{g,c}},\ -D^{\mathrm{eff}}_{\mathrm{i,gc}}\nabla C_{\mathrm{i,gc}}=h_{\mathrm{m}}(C_{\mathrm{i,gc}}-C_{i,\infty}),$$
$$i=\mathrm{O_2},\ \mathrm{Water\ Vapor},\ -k^{\mathrm{eff}}_{\mathrm{T}}\left.\frac{\partial T}{\partial x}\right|_{-}=h(T-T_{\infty}) \tag{30}$$

The heat transfer coefficient (h) and mass transfer coefficient (h_{m}) are taken from the natural convection correlations on a horizontal surface facing down [41,42]:

$$\begin{aligned}&\mathrm{Nu}=hL/k=0.27(\mathrm{Gr}\ Pr)^{0.25},\quad \mathrm{Gr}=g\beta\left|\Delta T\right|L^3/\nu^2\\&\mathrm{Sh}=h_{\mathrm{m}}L/D_{\mathrm{i,gc}}=0.27(\mathrm{Gr\ Sc})^{0.25},\quad \mathrm{Gr}=g\rho\left|\Delta\rho\right|L^3/\mu^2,\quad \mathrm{Sc}=\nu/D_{\mathrm{i,gc}}\end{aligned} \tag{31}$$

$x_1<x<x_2$ *and* $y=0$ *or* $y=y_1$: These two boundaries represent the gas CO_2 exits. Note that the mass transport of gases and heat transport between the surface and the ambient air are also through natural convection. The boundary conditions are given by:

$$p_{\mathrm{g,a}}=0,\quad -D^{\mathrm{eff}}_{\mathrm{i,ga}}\nabla C_{\mathrm{i,ga}}=h_{\mathrm{m}}(C_{\mathrm{i,ga}}-C_{i,\infty}),\quad i=\mathrm{Methanol\ Vapor,\ Water\ Vapor} \tag{32}$$

$x<x_1$ *or* $x>x_2$ *and* $y=0$ *or* $y=y_1$: These represent the solid walls of the vapor feed DMFC, and thus, the boundary conditions are specified as follows:

$$\frac{\partial\phi}{\partial y}=0,\quad \phi=C_{\mathrm{ML}},C_{\mathrm{MV,ga}},C_{\mathrm{WV,ga}},p_{\mathrm{l,a}},p_{\mathrm{g,a}},C_{\mathrm{O_2,gc}},C_{\mathrm{WV,gc}},p_{\mathrm{l,c}},p_{\mathrm{g,c}},\lambda \tag{33}$$

3.3. Sub-models

In order to fulfill the unified model, some sub-models for the electrochemical reactions as well as the interfacial transfer rates of water and methanol between liquid and vapor phases are indispensable.

On the DMFC anode, the kinetics of the methanol oxidation reaction (MOR) is modeled by the Tafel-like expression:

$$j_{\mathrm{a}}=A_{\mathrm{v,a}}j^{\mathrm{ref}}_{0,\mathrm{MeOH}}\left(\frac{C_{\mathrm{M}}}{C^{\mathrm{ref}}_{\mathrm{MeOH}}}\right)^{\gamma}\exp\left(\frac{\alpha_a F}{RT}\eta_a\right) \tag{34}$$

where the reaction order (γ) is related to the methanol concentration, and is assumed to be zero-order when methanol concentration is higher than a reference value [34]. Otherwise, the first-order reaction is applied.

The cell current density can be calculated by

$$I=\int_{\mathrm{ACL}}j_{\mathrm{a}}\ \mathrm{d}x \tag{35}$$

The rate of methanol crossover is expressed by the 'parasitic' current density:

$$I_{\mathrm{p}}=6FN_{\mathrm{MLcr}} \tag{36}$$

where the molar flux of methanol crossover (N_{MLcr}) is given by Eq. (19).

On the cathode, it is assumed that both the cell current and the 'parasitic' current are entirely consumed by the oxygen reduction reaction (ORR), i.e.:

$$I+I_{\mathrm{p}}=\int_{\mathrm{CCL}}j_{\mathrm{c}}\ \mathrm{d}x \tag{37}$$

where the ORR is also given by the Tafel-like expression:

$$j_{\mathrm{c}}=(1-s)A_{\mathrm{v,c}}j^{\mathrm{ref}}_{0,\mathrm{O_2}}\left(\frac{C_{\mathrm{O_2}}}{C^{\mathrm{ref}}_{\mathrm{O_2}}}\right)\exp\left(\frac{\alpha_c F}{RT}\eta_c\right) \tag{38}$$

In the above equation, $(1-s)$ accounts for the effect of liquid coverage in the cathode CL on the electrochemical reaction [34].

Table 2
Cell geometric dimensions and operating parameters.

Parameters	Symbols	Value	Unit
Vaporizer thickness	L	2.0×10^{-3}	m
Vapor transport layer thickness	x_2	2.0×10^{-3}	m
Gas exit	$x_2 - x_1$	0.5×10^{-3}	m
Anode diffusion layer thickness	$x_3 - x_2$	2.6×10^{-4}	m
Anode catalyst layer thickness	$x_4 - x_3$	0.2×10^{-4}	m
Membrane thickness (Nafion 115)	$x_5 - x_4$	1.25×10^{-4}	m
Cathode catalyst layer thickness	$x_6 - x_5$	0.2×10^{-4}	m
Cathode diffusion layer thickness	$x_7 - x_6$	2.6×10^{-4}	m
Air filter layer thickness	$x_8 - x_7$	1.0×10^{-3}	m
Width of the fuel cell	y_1	1.0×10^{-2}	m
Operation temperature	T	298	K
Anode liquid pressure in the tank	$p_{b,Tank}$	1.013×10^5	Pa
Ambient air pressure	$p^{\infty}_{g,c}$	1.013×10^5	Pa
Oxygen concentration in the ambient air	$C_{O_2,\infty}$	$0.21 \times p_g/RT$	mol m^{-3}

Finally, the cell voltage can be determined from:

$$V_{Cell} = V_0 - \eta_a - \eta_c - I\left(R_{Contact} + \frac{\delta_{mem}}{\sigma_{mem}}\right) \quad (39)$$

where V_0, $R_{Contact}$ and σ_{mem} mean the thermodynamic equilibrium voltage of the DMFC, the contact resistance and the proton conductivity of the membrane, respectively.

For the phase change between liquid water and water vapor, the rate of condensation and evaporation can be modeled using the finite-rate approach [30]:

$$\tilde{R}_{vl} = h_{vl}(y_{WV}p_g - p^{sat}_{WV}) \quad (40)$$

where p^{sat}_{WV} is the saturation pressure of water vapor, and y_{WV} is the molar fraction of water vapor in the gas phase. The mass-transfer coefficient (h_{vl}) can be given by [30]:

$$h_{vl} = \frac{k_c\varepsilon(1-s)y_{WV}}{2RT}\left(1+\frac{\left|y_{WV}p_g - p^{sat}_{WV}\right|}{y_{WV}p_g - p^{sat}_{WV}}\right) + \frac{k_e\varepsilon s\rho_l}{2M_{H_2O}}\left(1-\frac{\left|y_{WV}p_g - p^{sat}_{WV}\right|}{y_{WV}p_g - p^{sat}_{WV}}\right) \quad (41)$$

where k_c and k_e are the condensation and evaporation rate constants.

The rate of condensation and evaporation of methanol between liquid phase and vapor phase is modeled by the following expression [30]:

$$\tilde{R}_{MV,g} = A_{lg}h_{lg}s(1-s)\frac{(p^{sat}_{MV} - p_{MV})}{RT} \quad (42)$$

where p^{sat}_{MV} is the saturation pressure of methanol vapor.

The above-described governing equations for the cell geometric dimensions and operating parameters listed in Table 2 subjected to electrochemical properties listed in Table 3, were solved numerically by developing a simulation code, which was written based on the SIMPLE algorithm with the Finite-Volume-Method [30–33]. The grid independence of the present simulation model has also been fully investigated, and the grid with the number of 85×24 ($x \times y$) was used. The program was run on a desktop PC with an E8600 (3.33 GHz) Intel(R) Core(TM)2 Duo CPU. It typically took a dozen of hours and 2 million iterations to get converged results.

4. Results and discussion

4.1. General characteristics

To reveal the general mass transport characteristics during the working process of the passive vapor-feed DMFC, this section presents the two-dimensional distributions of species (e.g., methanol vapor, liquid methanol, water vapor, etc.) and temperature for the fuel cell discharged at a current density of 100 mA cm^{-2}. The ambient air has a temperature of 20 °C and a relative humidity

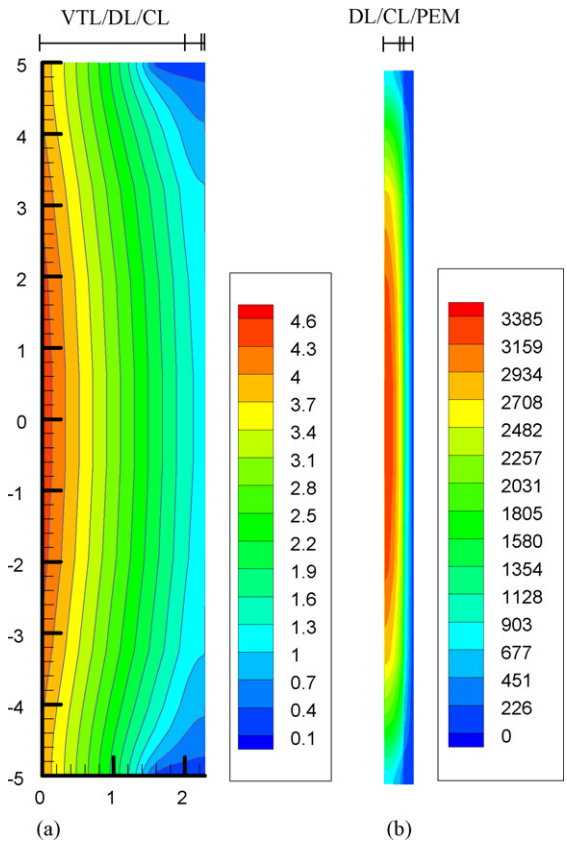

Fig. 4. Distribution of (a) concentration of methanol vapor (mol m^{-3}) in the anode VTL/DL/CL, and (b) concentration of methanol in liquid solution (mol m^{-3}) in the anode DL/CL/PEM.

of 50%. The concentration of methanol solution in the tank is 12 M and the open area ratio (A) of the vaporizer is 100%.

Fig. 4 shows the distributions of concentration of methanol vapor (in the anode VTL, DL and CL) and liquid methanol (in the anode DL, CL and PEM). For the distribution of methanol vapor concentration (Fig. 4a), it is seen that the methanol vapor shows the highest concentration (~3.9–4.5 mol m^{-3}) at the interface between the vaporizer and the VTL. This methanol vapor comes from the pervaporization of the liquid methanol solution (12 M) in the tank through the membrane vaporizer. It is also clear that the methanol vapor concentration decreases significantly along the VTL, anode DL and CL. For instance, the concentration decreases from 4.5 to 1.2 mol m^{-3} along the central line ($y = 0$). That clearly indicates the transport of methanol vapor through the VTL to the anode DL and CL, where it condenses into the liquid methanol solution. There is also some methanol vapor loss along with the gas CO_2 exhaust through the two gas exits, which accounts for the non-uniform distribution of methanol vapor along the y-direction. Note that the marked decrease (about 70%) of methanol vapor concentration through the VTL indicates the VTL can work effectively as a barrier layer for the methanol vapor transport. It is therefore anticipated that changing the properties of the VTL (e.g., thickness, porosity, permeability, etc.) can effectively adjust the distribution of methanol vapor concentration in the anode DL and CL.

Due to the condensation of methanol vapor, diluted methanol solution is formed in the anode DL and CL, as shown in Fig. 4b. The largest methanol concentration (about 3.4 M) comes from the surface of the anode DL, and it decreases through the DL and CL due to the electrochemical consumption of liquid methanol in the anode CL and the methanol crossover loss through the membrane to the cathode. The non-uniform distribution of liquid methanol

Table 3
Physicochemical properties used in the model.

Parameters		Symbols	Value	Unit	Ref.
Porosity, permeability	VTL	ε_{vtl}, K_{vtl}	0.3, 1.0×10^{-12}	–, m^2	–
	ADL	ε_{adl}, K_{adl}	0.75, 1.0×10^{-12}	–, m^2	–
	ACL	ε_{acl}, K_{acl}	0.3, 1.5×10^{-14}	–, m^2	[31]
	MEM	ε_{mem}, K_{mem}	0.3, 2.0×10^{-18}	–, m^2	[31]
	CCL	ε_{ccl}, K_{ccl}	0.3, 1.5×10^{-14}	–, m^2	[31]
	CDL	ε_{cdl}, K_{cdl}	0.75, 1.0×10^{-12}	–, m^2	–
	AFL	ε_{afl}, K_{afl}	0.7, 1.0×10^{-12}	–, m^2	–
Nafion volume fraction	ACL	$\varepsilon_{e,acl}$	0.3	–	–
	CCL	$\varepsilon_{e,ccl}$	0.3	–	–
Diffusivities	MeOH in water	$D_{M,l}$	$1.58\times10^{-9}e^{0.02623(T-298)}$	$m^2\,s^{-1}$	[31]
	MeOH in Nafion	$D_{M,N}$	$4.9\times10^{-10}e^{[2436(1/333-1/T)]}$	$m^2\,s^{-1}$	[31]
	MeOH in vaporizer	D_{pm}	$D_{M,N}$	$m^2\,s^{-1}$	Assumed
	Methanol vapor	$D_{M,g}$	$-6.954\times10^{-6}+4.5986\times10^{-8}T+9.4979\times10^{-11}T^2$	$m^2\,s^{-1}$	[31]
	O2 in gas	$D_{O_2,gc}$	$1.775\times10^{-5}\left(\frac{T}{273.15}\right)^{1.823}$	$m^2\,s^{-1}$	[31]
	Water vapor	$D_{WV,g}$	$2.56\times10^{-5}\left(\frac{T}{307.15}\right)^{2.334}$	$m^2\,s^{-1}$	[31]
	Dissolved water in Nafion	D_{we}	$4.17\times10^{-8}\lambda(161e^{-\lambda}+1)e^{-2436/T}$	$m^2\,s^{-1}$	[31]
Thermal conductivity of membrane		k_{mem}	0.2	$W\,m^{-1}\,K^{-1}$	[31]
Thermal conductivity of DL and CL		$k_{DL}(k_{CL})$	1.5	$W\,m^{-1}\,K^{-1}$	[31]
Thermal conductivity of VTL		k_{VTL}	1.5	$W\,m^{-1}\,K^{-1}$	[31]
Thermal conductivity of AFL		k_{AFL}	1.5	$W\,m^{-1}\,K^{-1}$	[31]
Thermal conductivity of gas		k_g	0.026	$W\,m^{-1}\,K^{-1}$	–
Thermal conductivity of liquid		k_l	0.62	$W\,m^{-1}\,K^{-1}$	–
Heat capacity of liquid water		c_{pl}	4200	$J\,kg^{-1}\,K^{-1}$	–
Heat capacity of gas		c_{pg}	1007	$J\,kg^{-1}\,K^{-1}$	–
Viscosity of gas phase		μ_g	2.03×10^{-5}	$kg\,m^{-1}\,s^{-1}$	[33]
Viscosity of liquid phase		μ_l	4.05×10^{-4}	$kg\,m^{-1}\,s^{-1}$	[33]
Absolute entropy of liquid methanol (1 atm, 298 K)		$\bar{s}^0_{MeOH,l}$	126.8	$J\,mol^{-1}\,K^{-1}$	–
Absolute entropy of liquid water (1 atm, 298 K)		$\bar{s}^0_{H_2O,l}$	69.95	$J\,mol^{-1}\,K^{-1}$	–
Absolute entropy of CO2 (1 atm, 298 K)		$\bar{s}^0_{CO_2}$	213.685	$J\,mol^{-1}\,K^{-1}$	–
Absolute entropy of O2 (1 atm, 298 K)		$\bar{s}^0_{O_2}$	205.033	$J\,mol^{-1}\,K^{-1}$	–
Electro-osmotic drag coefficients of water and methanol		n_{d,H_2O}	$\frac{2.5}{22}\lambda$	–	[31]
		$n_{d,M}$	$n_{d,H_2O}x_M$	–	–
Evaporation rate constant for water		k_e	5	$(atm\,s)^{-1}$	–
Condensation rate constant for water		k_c	5.0×10^4	s^{-1}	–
Interfacial transfer rate constant for methanol		h_{lg}	0.05	$m^2\,s^{-1}$	–
Specific interfacial area between liquid and gas		A_{lg}	105	m^{-1}	[33]
Proton conductivity in membrane		σ_{mem}	$7.3e^{[1268(1/298-1/T)]}$	$\Omega^{-1}m^{-1}$	[31]
Henry law constant for methanol		$k_{H,M}$	$0.096e^{0.04511(T-273)}$	atm	[31]
The saturation pressure of water vapor		$\log_{10}p^{sat}_{WV}$	$-2.1794+0.02953(T-273)-9.1837\times10^{-5}(T-273)^2+1.4454\times10^{-7}(T-273)^3$	atm	[31]
The saturation pressure of methanol vapor		p^{sat}_{MV}	$k_Hx_{M,l}$	atm	[31]
Latent heat of methanol evaporization		Δh_{Mv}	37.7×10^3	$J\,mol^{-1}$	–
Latent heat of water evaporization		Δh_v	44.9×10^3	$J\,mol^{-1}$	–
Thermodynamic voltage		V_0	1.21	V	[30]
Transfer coefficient of anode		α_a	0.52	–	[30]
Transfer coefficient of cathode		α_c	1.0	–	[30]
Anode exchange current density		$A_{v,a}j^{ref}_{0,M}$	$1\times10^5\exp\left(\frac{35{,}570}{R}\left(\frac{1}{353}-\frac{1}{T}\right)\right)$	$A\,m^{-3}$	[31]
Cathode exchange current density		$A_{v,c}j^{ref}_{0,O_2}$	$2111\exp\left(\frac{73{,}200}{R}\left(\frac{1}{353}-\frac{1}{T}\right)\right)$	$A\,m^{-3}$	[31]
Anode reference concentration		C^{ref}_M	100	$mol\,m^{-3}$	[33]
Cathode reference concentration		$C^{ref}_{O_2}$	36.5	$mol\,m^{-3}$	[33]
Surface tension		σ	0.0644	$N\,m^{-1}$	[33]
Membrane/aqueous phase partition coefficient		K	0.04	–	[33]
Equivalent weight of ionomer		EW	1.1	$kg\,mol^{-1}$	–
Dry membrane density		ρ_{dry}	1980	$kg\,m^{-3}$	–
Contact resistance		$R_{contact}$	0.45	$\Omega\,cm^2$	–

concentration along the *y*-direction is caused by the non-uniform distribution of methanol vapor concentration, as shown in Fig. 4a. The distribution of liquid methanol concentration in the anode CL and DL of the passive vapor-feed DMFC is very similar to that of a liquid-feed DMFC, which can be referred to [30–33]. Therefore, it is anticipated that the performance of this passive vapor-feed DMFC supplied with concentrated methanol solution of 12 M is similar to that of a liquid-feed DMFC fed with diluted methanol solution of 3.4 M, while clearly the energy density of the passive vapor-feed DMFC is higher.

To further reveal the presence of liquid methanol solution in the anode, the liquid saturation distribution in the *x*-direction at different *y*-locations is shown in Fig. 5. Due to the different properties of the different porous layers, there is only gas phase ($s=0$) in the hydrophobic VTL and AFL, while there are both liquid and gas phases ($0<s<1$) in the CL and DL which have mixed-wettability porous structures. Moreover, the liquid saturation remains nearly the same within each component (CLs and DLs), which indicates that liquid is confined within the CL and DL by the presence of the hydrophobic VTL in the anode side and the AFL in the cathode side.

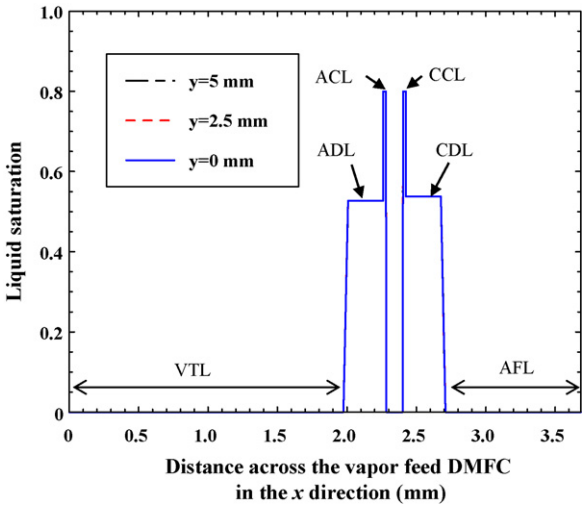

Fig. 5. Distribution of liquid saturation in the fuel cell in the x-direction at different y-locations.

Generally, it is clear from Figs. 4 and 5 that the working process of the passive vapor-feed DMFC involves complex physicochemical processes including the pervaporation of liquid methanol through the vaporizer, the transport of methanol vapor through the VTL towards the anode CL, the condensation of methanol vapor into the diluted liquid methanol solution, the transport of liquid methanol in the anode DL and CL, and the electrochemical consumption of liquid methanol in the anode CL.

Fig. 6 shows the distribution of water vapor concentration and temperature rise across the fuel cell. For the water vapor (Fig. 6a), the concentration in the anode side decreases from the CL towards the two gas exits, which means the water vapor comes by evaporation from liquid water in the anode CL and DL and is lost through the gas exits along with the gas CO_2. Therefore, sufficient water should be recovered from the cathode to the anode to make up for the water consumption in the anodic reaction and the water vapor loss with the gas CO_2 exhaust. At the cathode side, the water vapor concentration decreases from the CL to the surface of the AFL, indicating water vapor loss from the cathode side to the ambient air. For

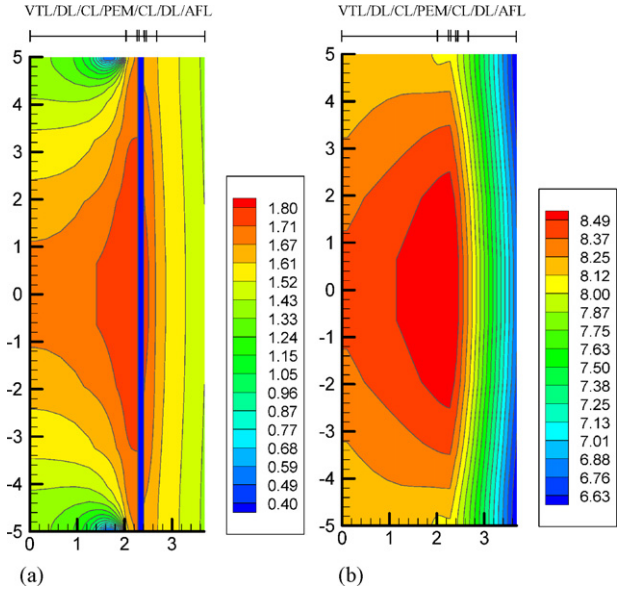

Fig. 6. Distribution of (a) concentration of water vapor (mol m^{-3}) in the anode VTL/DL/CL and cathode CL/DL/AFL, and (b) temperature rise (°C) across the fuel cell.

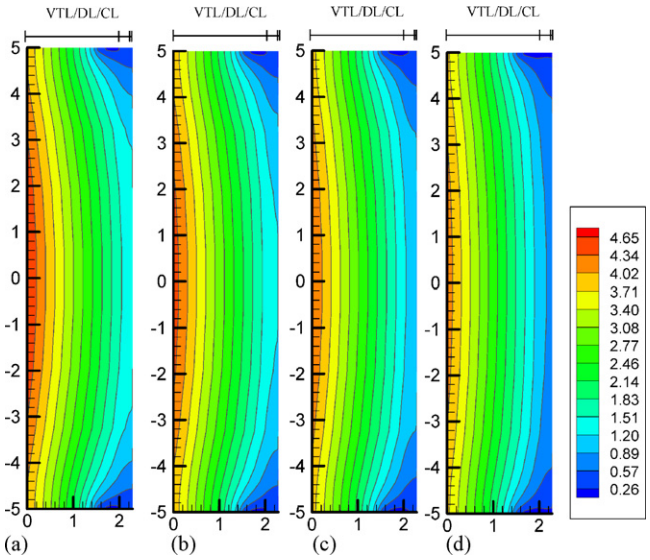

Fig. 7. Distribution of methanol vapor concentration (mol m^{-3}) in the anode VTL/DL/CL at different current densities: (a) 50 mA cm^{-2}, (b) 100 mA cm^{-2}, (c) 150 mA cm^{-2}, and (d) 200 mA cm^{-2}.

the temperature rise across the cell (Fig. 6b), it is seen that due to the heat generation within the cell, the cell temperature is 6.6–8.5 °C higher than the ambient temperature. The distribution of temperature is also non-uniform: it is higher within the cell while lower near the gas exits and the surface of the AFL, through which heat is dissipated to the ambient air. The largest temperature difference within the cell is about 1.9 °C.

4.2. Effect of cell current density

Fig. 7 shows the two-dimensional distributions of methanol vapor concentration in the anode VTL, DL and CL at current densities of 50, 100, 150 and 200 mA cm^{-2}. With the increase in current density, the methanol vapor concentration decreases within the whole region. The change of methanol vapor concentration with current density can be seen more clearly in Fig. 8, which shows the methanol vapor concentration in the x-direction at different y-locations for different current densities. It is seen that the methanol vapor concentration at the surface of the VTL decreases with the increase in current density. For instance, the concentra-

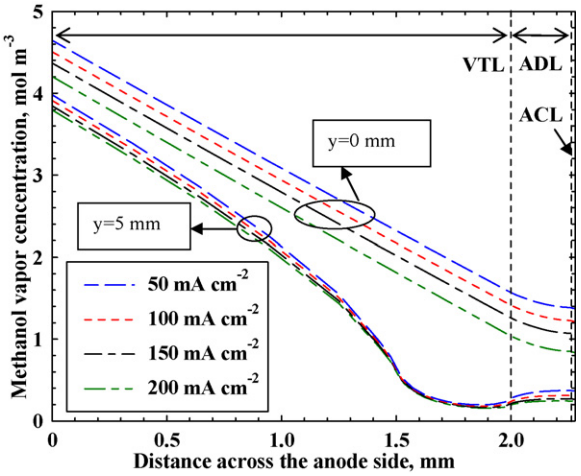

Fig. 8. Distribution of methanol vapor concentration in the anode VTL/DL/CL at different y-coordinates and at different current densities.

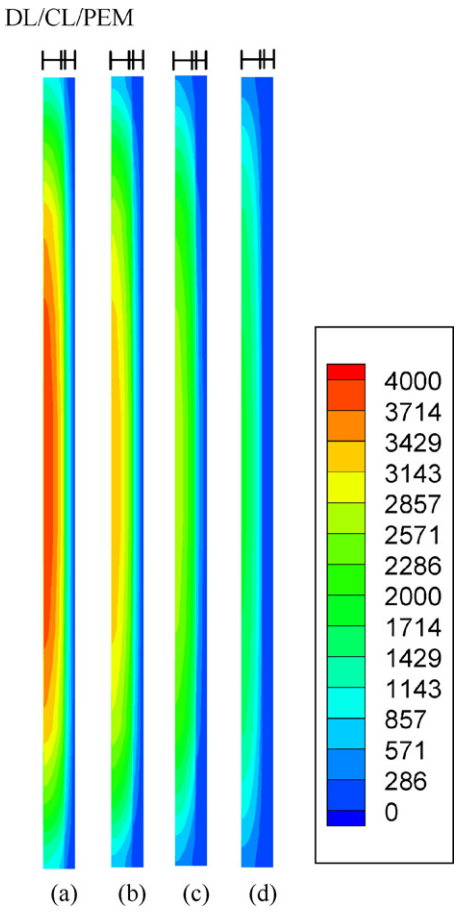

Fig. 9. Distribution of liquid methanol concentration (mol m^{-3}) in the DL/CL/PEM at different current densities: (a) 50 mA cm^{-2}, (b) 100 mA cm^{-2}, (c) 150 mA cm^{-2}, and (d) 200 mA cm^{-2}.

tion at the middle of the surface decreases from 4.65 to 4.2 mol m^{-3} when the current density is increased from 50 to 200 mA cm^{-2}. That is because, from Eq. (2), the larger methanol generation rate requested by the increased current density leads to a lower methanol vapor concentration on the surface of the VTL. At the same time, the methanol vapor concentration within the whole region decreases with the current density. Near the side wall (y = 5 mm), the methanol vapor concentration first decreases, and then increases after the location of the gas exit, which indicates

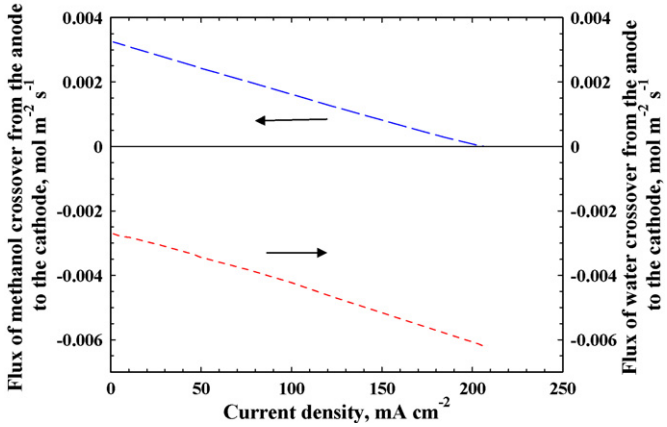

Fig. 10. Molar flux of methanol and water crossover from the anode to the cathode with the increase in current density.

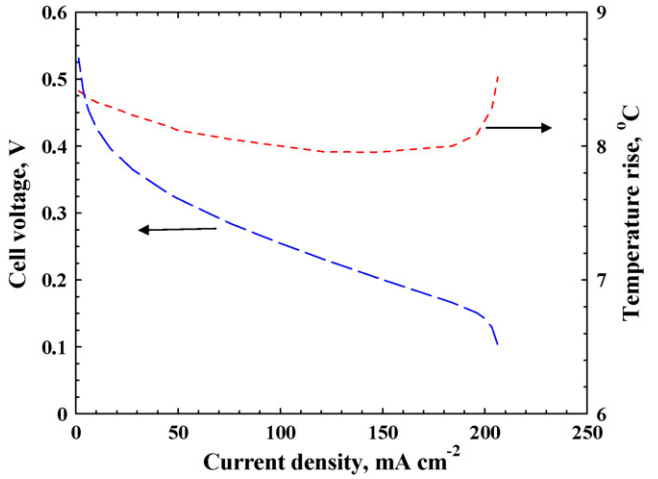

Fig. 11. Cell performance of the vapor-feed DMFC and the variation in the average cell temperature rise with the increase in current density.

some methanol vapor loss through the gas exit. Since the methanol vapor concentration is relatively lower in the DL and CL, the locations of gas exits are chosen to be near the DL in order to reduce the vapor loss through the gas exits.

The distributions of methanol concentration in the liquid solution at different current densities are shown in Fig. 9. It is clear that the liquid methanol concentration decreases in the whole region with the increase in current density. The methanol concentration at the surface of the anode DL decreases from about 4.0 to 1.8 M when the current density increases from 50 to 200 mA cm^{-2}. The decrease in methanol concentration with current density leads to a decrease in methanol crossover through the membrane, which can be seen in Fig. 10. With the increase in current density, the methanol crossover is seen to decrease nearly linearly from about 0.0032 mol m^{-2} s^{-1} to almost 0, at which a limiting current density occurs.

The current density also influences the water crossover through the membrane, which can also be seen in Fig. 10. It is seen that the flux of water crossover from the anode to the cathode is negative, meaning the water crossover is from the cathode to the anode, and the flux of water crossover from the cathode to the anode increases with current density. The "negative" water crossover results from the reduction of water flux by diffusion from the anode to the cathode, and from the significant increase in the water flux by convection from the cathode to the anode caused by the hydrophobic AFL [31,32]. With the increase in current density, more liquid water is generated in the cathode CL, and higher liquid pressure is built up in the cathode, which pushes more water to the anode through the membrane. The increased water crossover happens to make up for the increased water consumption in the anode with current density. It is worth pointing out that the change of water crossover through the membrane with current density for the passive vapor-feed DMFC is similar to that of a passive liquid-feed DMFC, which has been presented elsewhere [30–32].

The polarization curve of the passive vapor-feed DMFC is shown in Fig. 11. Similar to a liquid-feed DMFC, the cell voltage decreases with the increase in current density. There is a rapid drop in cell voltage when the current density approaches 208 mA cm^{-2}, which is the limiting current density caused by large mass transport polarization. The cell performance gives a peak power density of about 30 mW cm^{-2} at the cell voltage of 0.2 V, which is similar to a passive liquid-feed DMFC fed with 3 M [32]. Fig. 11 also shows the variation in the average cell temperature rise with the increase in current density. The average cell temperature at any current density is always above the ambient temperature due to the heat generation

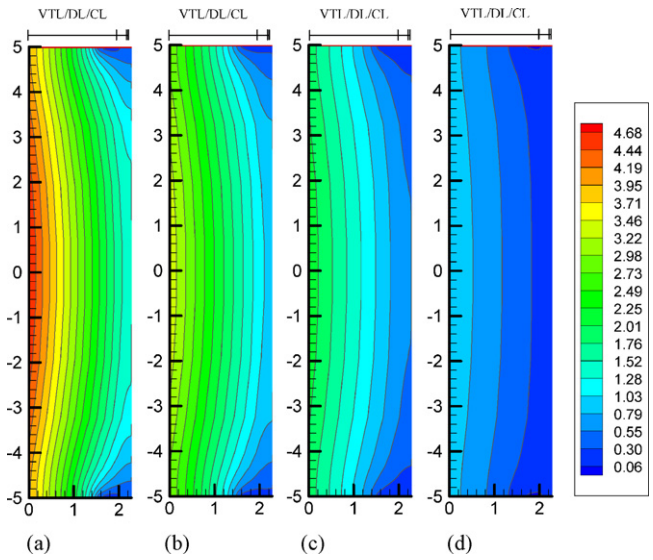

Fig. 12. Distribution of methanol vapor concentration (mol m^{-3}) in the anode VTL/DL/CL at current densities of 40 mA cm^{-2}, with different vaporizer open area ratios: (a) 100%, (b) 75%, (c) 50%, and (d) 25%.

caused by the electrochemical reaction. However, the average cell temperature rise first decreases slightly and then increases with the current density. That behavior is different from that of a passive liquid feed DMFC, which shows a continuous increase in temperature with current density [31,32]. The first decrease in cell temperature is possibly due to the significant decrease of liquid methanol concentration in the anode with current density (as shown in Fig. 9), which lowers the methanol crossover and leads to a reduced heat generation caused by methanol crossover.

4.3. Effect of open area ratio of the vaporizer

As mentioned above, the vapor generation rate across the vaporizer, as well as the concentration of methanol vapor at the membrane–vapor interface, can be controlled by adjusting the open area ratio of the vaporizer. In this section, different open area ratios (100%, 75%, 50% and 25%) for the passive vapor-feed DMFC fed with 12 M concentrated solution in the tank were tested. Fig. 12 shows the distributions of methanol vapor concentration for a cell operating at 40 mA cm^{-2} with different vaporizer open area ratios. It is seen that the methanol vapor concentration decreases greatly in the whole anode region with the decrease in the open area ratio. The maximum methanol vapor concentration (at the center of the surface of the VTL) decreases from about 4.68 to 0.99 mol m^{-3} when the open area ratio is decreased from 100% to 25%. Therefore, adjusting the open area ratio of the vaporizer can effectively change the methanol vapor concentration in the anode porous region, which significantly affects the liquid methanol concentration in the anode DL and CL. The distributions of liquid methanol concentration with different open area ratios are shown in Fig. 13. With the decrease in the open area ratio, the liquid methanol concentration clearly decreases. For instance, the maximum liquid methanol concentration (at the center of the surface of the anode DL) decreases greatly from about 4.1 to 0.6 M. That clearly shows that the liquid methanol concentration in the anode DL and CL can be effectively controlled by changing the open area ratio of the vaporizer.

The decrease in the liquid methanol concentration with the decrease in the vaporizer open area ratio also influences the flux of methanol and water through the membrane, which is shown in Fig. 14. The flux of methanol crossover decreases with the decrease

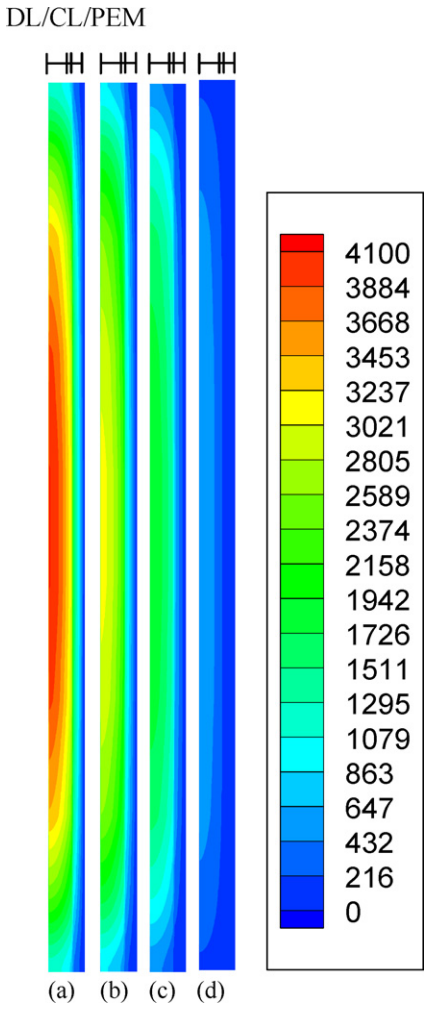

Fig. 13. Distribution of liquid methanol concentration (mol m^{-3}) in the DL/CL/PEM at current densities of 40 mA cm^{-2}, with different vaporizer open area ratios: (a) 100%, (b) 75%, (c) 50% and (d) 25%.

in the open area ratio due to the reduced liquid methanol concentration. For the flux of water crossover through the membrane from the cathode to the anode, it also decreases with the decrease in the open area ratio. That is because the reduced methanol crossover lowers the water generation rate in the cathode CL, and thus less water is pushed to the anode through the membrane.

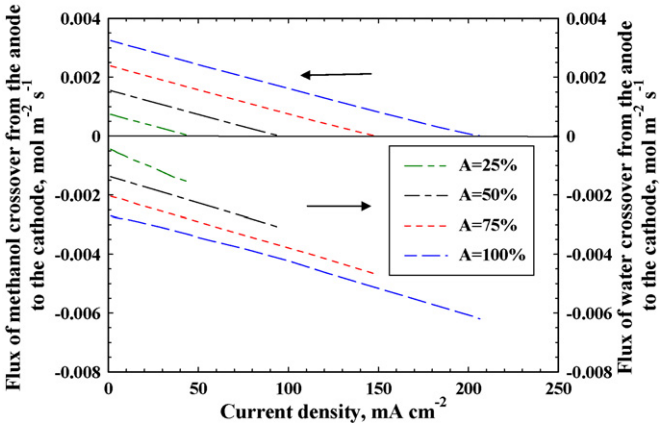

Fig. 14. Molar flux of methanol and water crossover from the anode to the cathode with the increase in current density with different vaporizer open area ratios.

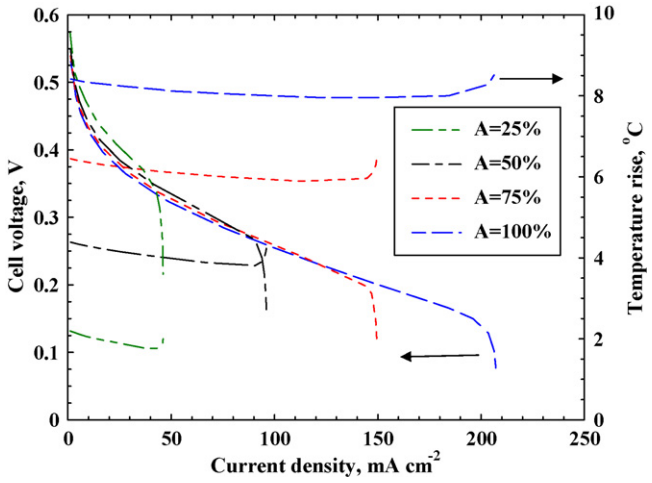

Fig. 15. Cell performance of the passive vapor-feed DMFC and the variation in the average cell temperature rise with the increase in current density with different vaporizer open area ratios.

Both the cell performance and the variation in the average cell temperature rise with the increase in current density for different open area ratios are shown in Fig. 15. With the decrease in the open area ratio, the cell voltage increases in the low current density region, while the limiting current density decreases nearly proportionally due to the lowered liquid methanol concentration in the anode. The observation about the effect of vaporizer open area ratio on the cell performance agrees well with the experimental finding by Eccarius et al. [7]. For the average temperature rise, it always decrease slightly first and then increases with current density for different open area ratios, while it is decreased evidently with the decrease in the open area ratio. The average temperature rise near the open-circuit condition ($i = 0$) decreases from about 8.5 to 2.5 °C when the open area ratio decreases from 100% to 25%. That is because the heat generation caused by the methanol crossover is significantly lowered.

4.4. Effect of methanol concentration in the tank

From Eq. (2), it is clear that fixing the open area ratio of the vaporizer (A) while changing the methanol concentration in the tank ($C_{ML,Tank}$) yields the same results as fixing ($C_{ML,Tank}$) while changing A, if $A \times C_{ML,Tank}$ is constant. For example, $C_{ML,Tank} = 24M$ (neat methanol) and $A = 50\%$ gives the same results as $C_{ML,Tank} = 12$ M and $A = 100\%$, which have been discussed in preceding sections. Therefore, the effect of methanol concentration in the tank can be directly drawn from the proceeding sections. Main results are listed as follows:

(1) For a fixed open area ratio and a given current density, an increase in the tank methanol concentration results in an increase in methanol vapor concentration in the VTL, anode DL and CL, which finally leads to an increase in liquid methanol concentration in the anode DL and CL. Accordingly, the flux of methanol crossover from the anode to the cathode, and water crossover from the cathode to the anode all increases with the methanol concentration in the tank.
(2) With an increase in the tank methanol concentration, the cell voltage is lowered slightly in the low current density region, while the mass transport polarization is reduced and the limiting current density is increased. The cell temperature also increases with the methanol concentration in the tank.

Therefore, it is clear that the mass transport and cell performance of the passive vapor-feed DMFC depend highly on both the open area ratio of the vaporizer and the methanol concentration in the tank. Theoretically, increasing the methanol concentration in the tank, and optimizing the vaporizer open area ratio, could achieve the maximum cell performance as well as the largest energy density of the system.

5. Conclusions

Based on a two-dimensional, two-phase, non-isothermal model using the multi-fluid approach, the mass transport in the passive vapor-feed DMFC, as well as the effects of various operating parameters and cell structures on the mass transport and cell performance, were numerically investigated. The model features the consideration of vapor generation through a membrane vaporizer and the vapor transport through a hydrophobic vapor transport layer. The results show that the passive vapor-feed DMFC involves complex physicochemical processes including pervaporation of liquid methanol through the vaporizer, transport of methanol vapor through the hydrophobic vapor transport layer towards the anode electrode, condensation of methanol vapor into the diluted methanol solution, transport of liquid methanol within the anode diffusion layer and catalyst layer, and electrochemical consumption of liquid methanol in the anode catalyst layer. It is also shown that the passive vapor-feed DMFC supplied with concentrated methanol solution or neat methanol can yield similar performance with the liquid-feed DMFC fed with much diluted methanol solution, while giving a higher system energy density. The mass transport and cell performance of the vapor-feed DMFC are found to depend highly not only on the current density, but also on the open area ratio of the vaporizer and the methanol concentration in the tank. Therefore, the maximum cell performance, as well as the largest energy density of the system, can be achieved by increasing the methanol concentration in the tank and optimizing the open area ratio of the vaporizer.

Acknowledgement

The financial support from National Science Foundation (Contract No. CBET-0730349) is gratefully acknowledged.

References

[1] C.K. Dyer, J. Power Sources 106 (2002) 31–34.
[2] C. Xu, T.S. Zhao, J. Power Sources 168 (2007) 143–153.
[3] Z. Guo, A. Faghri, J. Power Sources 160 (2006) 1183–1194.
[4] T.S. Zhao, C. Xu, R. Chen, W.W. Yang, Prog. Energy Combust. Sci. 35 (2009) 275–292.
[5] J. Lobato, P. Canizares, M.A. Rodrigo, J.J. Linares, R. Lopez-Vizcaino, Energy Fuels 22 (2008) 3335–3345.
[6] I. Chang, S. Ha, S. Kim, S. Kang, J. Kim, K. Choi, S.W. Cha, J. Power Sources 188 (2009) 205–212.
[7] S. Eccarius, F. Krause, K. Beard, C. Agert, J. Power Sources 182 (2008) 565–579.
[8] S. Eccarius, X. Tian, F. Krause, C. Agert, J. Micromech. Microeng. 18 (2008), 104010 (9pp).
[9] H. Kim, J. Power Sources 162 (2006) 1232–1235.
[10] J. Rice, A. Faghri, Int. J. Heat Mass Transfer 51 (2008) 948–959.
[11] A.K. Shukla, P.A. Christensen, A. Hamnett, M.P. Hogarth, J. Power Sources 55 (1995) 87–91.
[12] A.S. Arico, P. Creti, H. Kim, R. Mantegna, N. Giordano, V. Antonucci, J. Electrochem. Soc. 143 (1996) 3950–3959.
[13] M. Hogarth, P. Christensen, A. Hamnett, A. Shukla, J. Power Sources 69 (1997) 125–136.
[14] K. Scott, W.M. Taama, P. Argyropoulos, J. Power Sources 79 (1999) 43–59.
[15] J. Kallo, W. Lehnert, R.V. Helmolt, J. Electrochem. Soc. 150 (2003) A765–A769.
[16] H. Fukunaga, T. Ishida, N. Teranishi, C. Arai, K. Yamada, Electrochim. Acta 49 (2004) 2123–2129.
[17] Z. Guo, A. Faghri, J. Power Sources 167 (2007) 378–390.
[18] A. Faghri, Z. Guo, Appl. Therm. Eng. 28 (2008) 1614–1622.
[19] I. Chang, S. Ha, J. Kim, J. Lee, S.W. Cha, J. Power Sources 184 (2008) 9–15.
[20] L. Yang, W.C. Huang, U.S. Patent Pub. No. 2005/0164059A1.

[21] R.S. Hirsch, P.F. Mutolo, J.J. Becerra, R.K. Sievers, J.P. Scartozzi, W.P. Acker, U.S. Patent Pub. No. 2004/0209133A1.
[22] J.A. Drake, A.G. Gilicinski, G.G. Guay, L.J. Pinnell, U.S. Patent Pub. No. 2005/0058874A1.
[23] X. Ren, J.J. Becerra, R.S. Hirsch, S. Gottesfeld, F.W. Kovacs, K.J. Shufon, U.S. Patent Pub. No. 2005/0170224A1.
[24] X. Ren, F.W. Kovacs, K.J. Shufon, S. Gottesfeld, U.S. Patent Pub. No. 2008/0032182A1.
[25] H.K. Kim, J.M. Oh, J.Y. Lee, H. Chang, U.S. Patent Pub. No. 2006/0269825 A1.
[26] X. Ren, J.J. Becerra, R.S. Hirsch, S. Gottesfeld, F.W. Kovacs, K.J. Shufon, U.S. Patent No. 7407721B2.
[27] B. Xiao, A. Faghri, Int. J. Heat Mass Transfer 52 (2009) 3525–3533.
[28] G. Jewett, Z. Guo, A. Faghri, Int. J. Heat Mass Transfer 52 (2009) 4573–4583.
[29] A. Faghri, Z. Guo, U.S. Patent No. US7625649B1.
[30] C. Xu, T.S. Zhao, W.W. Yang, J. Power Sources 178 (2008) 291–308.
[31] C. Xu, A. Faghri, Int. J. Heat Mass Transfer 53 (2010) 1951–1966.
[32] C. Xu, A. Faghri, J. Fuel Cell Sci. Technol 7 (2010), in press.
[33] W.W. Yang, T.S. Zhao, Electrochim. Acta 52 (2007) 6125–6140.
[34] Z.H. Wang, C.Y. Wang, J. Electrochem. Soc. 150 (2003) A508–A519.
[35] W.P. Liu, C.Y. Wang, J. Electrochem. Soc. 154 (2007) B352–B361.
[36] J. Rice, A. Faghri, Int. J. Heat Mass Transfer 49 (2006) 4804–4820.
[37] L. Li, Z. Xiao, S. Tan, L. Pu, Z. Zhang, J. Membr. Sci. 243 (2004) 177–187.
[38] T.V. Nguyen, G. Lin, H. Ohm, X. Wang, Electrochem. Solid-State Lett. 11 (2008) B127–B131.
[39] Q. Ye, T.V. Nguyen, J. Electrochem. Soc. 154 (2007) B1242–B1251.
[40] H. Meng, J. Power Sources 168 (2007) 218–228.
[41] J. Rice, A. Faghri, J. Heat Transfer 130 (2008) 062001.
[42] A. Faghri, Y. Zhang, Transport Phenomena in Multiphase Systems, Elsevier Inc., 2006.